

Mechanical Properties and Fracture Patterns of Pentagraphene Membranes

J. M. de Sousa^{1,2,3,*}, A. L. Aguiar², E. C. Girão², A. F. Fonseca¹, A. G. Souza
Filho³, and Douglas S. Galvao^{1,*,†}

^{†1}*Instituto de Física Gleb Wataghin, Universidade Estadual de Campinas, 13083-970,
Campinas, SP, Brazil.*

^{‡2}*Departamento de Física, Universidade Federal do Piauí, Teresina, Piauí, 64049-550,
Brazil*

^{¶3}*Departamento de Física, Universidade Federal do Ceará, P.O. Box 6030, CEP
60455-900, Fortaleza, Ceará, Brazil.*

E-mail: galvao@ifi.unicamp.br;josemoreiradesousa@gmail.com

Abstract

Recently, a new two-dimensional carbon allotrope called pentagraphene (PG) was proposed. PG exhibits mechanical and electronic interesting properties, including typical band gap values of semiconducting materials. PG has a Cairo-tiling-like 2D lattice of non coplanar pentagons and its mechanical properties have not been yet fully investigated. In this work, we combined density functional theory (DFT) calculations and reactive molecular dynamics (MD) simulations to investigate the mechanical properties and fracture patterns of PG membranes under tensile strain. We show that PG membranes can hold up to 20% of strain and that fracture occurs only after substantial dynamical bond breaking and the formation of 7, 8 and 11 carbon rings and carbon chains. The stress-strain behavior was observed to follow two regimes, one exhibiting

linear elasticity followed by a plastic one, involving carbon atom re-hybridization with the formation of carbon rings and chains. Our results also show that mechanically induced structural transitions from PG to graphene is unlikely to occur, in contrast to what was previously speculated in the literature.

Introduction

Graphene is one of the most important topics in materials science today.¹⁻⁸ Several studies have focused on physical and/or chemical modifications of the perfect honeycomb lattice, since its zero band gap value limits the development of some pure graphene-based digital electronic devices.⁹ Functionalization of graphene^{10,11} and graphene nanoribbons¹² are examples of strategies used to tune the band gap, but which has achieved only partial success. Due to of this, there is a renewed interest on other layered structures which have a band gap. Hexagonal boron-nitride,^{13,14} carbon nitride nanosheets,¹⁵⁻¹⁷ metal dichalcogenides,^{23,24} and silicene membranes²⁵⁻²⁷ are examples of other two-dimensional structures that overcome graphene “*bandgapless*” limitation. Other pure carbon structures such as graphynes¹⁸⁻²² and haeckelites²⁸ are also good candidates.

Recently, a new 2D carbon allotrope called *pentagraphene* (PG) (see Figure 1) has been proposed by Zhang *et al.*²⁹ Based on DFT calculations, they showed that such membranes have a unique arrangement of carbon atoms in a network of non-coplanar pentagons, similar to a *Cairo pentagonal tiling*. They also showed that PG is not only mechanically and thermodynamically stable, but also presents a large band gap of 3.25eV.²⁹ Besides that, PG also exhibits interesting thermal and mechanical properties, such as negative Poisson’s ratio (auxetic behaviour³⁰) due to its metastability and intricate atomic structural configuration. Figure 1 shows PG frontal and a side view.

Several theoretical studies have been already devoted to PG and its stability has been the subject of debate.³¹ Some first-principles studies suggest PG is stable and described some of their electronic and mechanical properties.^{32,33} PG thermal conductivity at room

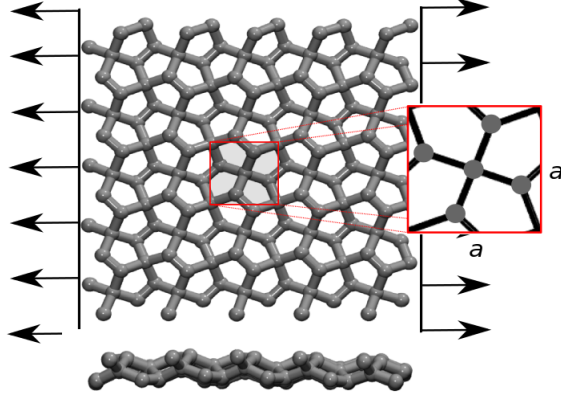


Figure 1: Frontal (top) and lateral (bottom) views of a pentagraphene (PG) membrane. The arrows indicate the directions of the applied tensile deformations considered in this study. The figure inset shows the PG square unit cell, with lattice parameter $a = 3,64 \text{ \AA}$.

temperature has been estimated by different methods to be about 167 W/mK^{34} (from MD simulations) and 645 W/mK^{35} (from first principles calculations). PG nanoribbons have also been theoretically investigated in terms of stability and electronic band structure. These quasi-1D systems have been shown to preserve the semiconducting character from their layer parent counterpart and the gap value depends on width.³⁶ Similar to graphene, PG functionalization (hydrogenation and fluorination) allows the tuning of its electronic and mechanical properties,³⁸ and an unexpected increase in thermal conductivity was observed in the hydrogenation case.³⁹ Recently, interesting PG mechanical and structural behaviors were reported based on reactive molecular dynamics (MD) simulations.⁴⁰ It has been predicted that a structural transition from PG to graphene (or from PG to hexagraphene) can occur as a result of thermal and/or tensile strains, thus leading to the assumption that PG and graphene might be considered different structural phases of the same material.⁴⁰

In this paper, we combine density functional theory (DFT) calculations and reactive classical MD simulations (with a properly chosen set of potential parameters) to investigate the fracture patterns of PG membranes under axial tensile strain, as schematically shown in Fig. 1. Differently from the conclusions of Ref.,⁴⁰ our results reveal the formation of structures with 7, 8 and 11 carbon rings and carbon chains, just before the mechanical failure (fracture), which happens at about 20% of strain. Both Young's modulus and Poisson's ratio

of PG were also calculated and compared with the original *ab initio* predictions.²⁹

Methods

We combined quantum (DFT) and classical (MD) methods to investigate the structural and dynamical aspects of PG membranes under tensile strain, up to the limit of mechanical failure (fracture). In the following sections we provide technical details on the computational techniques used in this paper.

DFT calculations

We used a LCAO-based DFT approach,^{41,42} as implemented in the SIESTA code.^{43,44} The Kohn-Sham orbitals were expanded in a double- ζ basis set composed of numerical pseudoatomic orbitals of finite range enhanced with polarization orbitals. A common atomic confinement determined by an energy shift of 0.02 Ry was used to define the cutoff radius for the basis functions, while the fineness of the real space grid was determined by a mesh cutoff of 400 Ry.⁴⁹ For the exchange-correlation potential, we used the generalized gradient approximation (GGA),⁴⁵ and the pseudopotentials were modeled within the norm-conserving Troullier-Martins⁴⁶ scheme in the Kleinman-Bylander⁴⁷ factorized form. Brillouin-zone integrations were performed by using a Monkhorst-Pack⁴⁸ grid of $8 \times 8 \times 1$ k -points. All geometries were fully optimized for each strain level until the maximum force component on any atom was less than 10 meV/Å. The lattice vectors were manually deformed along selected directions (uniaxial and biaxial) and the coordinates of carbon atoms were rescaled along these directions before fully convergence. For uniaxial stretching, we have considered two cases: with and without constrains along the perpendicular directions. The stress tensor σ_{ij} is related to strain tensor ε_{ij} ($i, j = x, y, z$) by $\sigma_{ij} = (1/S)(\partial U / \partial \varepsilon_{ij})$, where $S = (\vec{a}_x \times \vec{a}_y)$ is the area of the unit cell. For each strained structural geometry relaxation, the SCF convergence thresholds for electronic total energy were set to 10^{-4} eV. Periodic boundary

conditions were imposed, with a perpendicular off-plane lattice vector a_z large enough (20 Å) to prevent spurious interactions between periodic images.

MD simulations

The MD simulations were performed using the reactive force field (ReaxFF).^{50,51} The numerical integration of the Newton’s equations was performed in the large-scale atomic / molecular massively parallel simulator (LAMMPS) code.⁵² ReaxFF is a reactive force field developed by van Duin, Goddard III and co-workers, which is designed to be a bridge between quantum chemical force fields and empirical bonding energy terms. ReaxFF is parameterized using available experimental data and/or using DFT calculations. In ReaxFF, the total bond energy between atoms are obtained through the computation of all interatomic distances and updated at every time step of the classical MD runs. In this way, the structural connectivity is determined uniquely by the atomic positions, thus allowing the ReaxFF to create and break (dissociate) chemical bonds in a dynamical way, through the whole simulation. This is important to describe not only the equilibrium structures, but also the fracture patterns of the investigated systems. The energy of the system is divided into partial energy contributions, which include bonded and non-bonded terms as follows :⁵⁰

$$\begin{aligned}
 E_{system} = & E_{bond} + E_{over} + E_{under} + E_{val} \\
 & + E_{pen} + E_{tor} + E_{conj} + E_{vdW} \\
 & + E_{co} \quad , \quad (1)
 \end{aligned}$$

where each term, respectively, represents the energies corresponding to the bond distance, the over-coordination, the under-coordination, the valence, the penalty for handling atoms with two double bonds, the torsion, the conjugated bond energies, the van der Waals, and coulomb interactions, respectively.

ReaxFF has been extensively used in the study of the dynamic aspects of nanostruc-

tures, such as fractures of graphynes,⁵³ silicene membranes,⁵⁴ connected carbon nanorings,⁵⁵ carbyne,^{56,57} the degradation of graphene and graphdiyne membranes in gaseous atmospheres,^{58,59} among other carbon based nanostructures.

Here, for the study of structural and fracture mechanics of PG structures, we considered square membranes under periodic boundary conditions with dimensions of approximately $80 \text{ \AA} \times 80 \text{ \AA}$. In all calculations, these structures were initially thermalized at 300 K in a NPT ensemble, in order to obtain a structure corresponding to zero external pressure, before the beginning of the fracture dynamics study. After that, a stretching process was then considered within a NVT ensemble, also at 300 K, with the temperature set controlled by a Nose-Hoover thermostat,⁶⁰ as implemented in the LAMMPS⁵² code.

In our calculations, the timestep of numerical integration was set to 0.05 fs and a constant strain rate of 10^{-6} fs^{-1} was considered. The above conditions were maintained up to the mechanical failure limit. The PG mechanical properties were analyzed by the stress-strain relationship, where the engineering strain, ε , under tension is defined as

$$\varepsilon = \frac{\zeta - \zeta_0}{\zeta_0} = \frac{\Delta\zeta}{\zeta_0}, \quad (2)$$

where ζ_0 and ζ are the length of the structure before and after the dynamics of deformation, respectively. The *per-atom* stress tensor of each carbon atom are calculated by:⁶¹

$$\sigma_{\alpha\beta} = \frac{1}{\Gamma} \sum_i^N (m_i v_{\alpha i} v_{i\beta} + r_{i\alpha} f_{i\beta}), \quad (3)$$

where Γ is the atom volume, N the number of atoms, m_i the mass of carbon atoms, v the velocity, r the coordinates of the carbon atoms and $f_{i\beta}$ is the β component of the force acting on the i -th atom. In order to perform a more detailed analysis of the distribution of stress along the structure during the fracture process, we also calculated the quantity known as

von Mises stress, σ_{vM} , which is mathematically given by:⁶¹

$$\sigma_{vM} = \left[\frac{(\sigma_{xx} - \sigma_{yy})^2 + (\sigma_{yy} - \sigma_{zz})^2 + (\sigma_{zz} - \sigma_{xx})^2 + (\sigma_{xy} + \sigma_{yz} + \sigma_{zx})^2}{2} \right]^{\frac{1}{2}}, \quad (4)$$

where σ_{xy} , σ_{yz} and σ_{zx} are shear stress components. The von Mises stress has been used in the mechanical studies of other nanostructures as silicene membranes⁵⁴ and carbon nanotubes unzipping.⁶² It is very useful to visualize how the stress accumulates and dissipates during the stretching/fracture processes.

Results

Choice of ReaxFF parameters

Before starting the MD study of PG fractures, we performed DFT- and MD-based calculations tests to use as benchmark for the choice of the multiple available ReaxFF set parameters. Among the possible choices, we considered four different ReaxFF sets, as developed by Mueller *et al.*,⁵¹ Mattsson *et al.*,⁶³ Chenoweth *et al.*,⁶⁴ and Srinivasan *et al.*⁶⁵ These parameters were developed for carbon in different multicomponent systems. The one from Srinivasan, for instance, was recently developed for condensed phases of carbon. The tests consist in the calculation of the thickness, the Young's modulus, Y , and Poisson's ratio, ν , of PG structures using the same protocols by Zhang *et al.*²⁹ to estimate the elastic constants C_{11} and C_{12} , and also using the following equations:

$$Y = \frac{C_{11}^2 - C_{12}^2}{C_{11}}, \quad (5)$$

and

$$\nu = \frac{C_{12}}{C_{11}}. \quad (6)$$

The elastic constants C_{11} and C_{12} were obtained from energy minimization calculations of the structure in uniaxial and biaxial tensile strains, respectively. Uniaxial simulations, (as shown in Fig. 1), are made by fixing one dimension and applying strain along the other direction. Biaxial tensile strain consists of applying the same amount of strain along x and y directions at the same time. The energy minimizations were calculated with convergence tolerances of 0 and 10^{-8} for the energy and force, respectively.

In Table (1) we present the results previously reported in Ref.²⁹ for Y and ν , as well as the DFT and ReaxFF (four different set parameters) results obtained in our simulations. From this table we can see a good agreement between our DFT (performed with a localized

Table 1: Comparison of structural and mechanical properties of pentagraphene (PG) structures obtained from DFT,²⁹ our DFT calculations, and ReaxFF.^{51,63-65}

Method	Thickness (Å)	Young's Modulus (GPa.nm)	Poisson's ratio
DFT from Ref. ²⁹	1.20	263.8	-0.068
DFT from our calculations	1.23	257.6	-0.096
ReaxFF - Mattsson ⁶³	0.882	150.5	-0.154
ReaxFF - Srinivasan ⁶⁵	1.34	133.9	0.366
ReaxFF - Muller ⁵¹	1.05	322.0	0.335
ReaxFF - Chenoweth ⁶⁴	1.09	197.0	0.380

orbital basis) results and those from Ref.²⁹ (which used a plane-wave basis set), including the prediction of the auxetic behavior. We then tested the different ReaxFF sets in order to determine which one provides the best results in comparison to the DFT ones, in terms of structural and mechanical properties. We observe that the Mattsson⁶³ set of parameters is the only one which correctly predicts the sign of PG Poisson's ratio. However, it presents a much softer structure (smaller thickness and modulus than those calculated from DFT). The Srinivasan⁶⁵ set of parameters predicts reasonable thickness but a much smaller elastic modulus than that from DFT. On the other hand, the Mueller⁵¹ and the Chenoweth⁶⁴ sets of parameters present the best matches for the thickness and Young's modulus as compared with both DFT calculations. If we take the results from Zhang *et al.*²⁹ as reference, both

Mueller’s and the Chenoweth’s sets give smaller thickness with similar deviations. On the other hand, those two parameter sets show distinct trends for the Young’s Modulus: Y is $\sim 22\%$ higher for Muller’s and $\sim 25\%$ lower for Chenoweth’s in comparison with Zhang’s DFT result. For the physical phenomenon aspects we are investigating here, the thickness and Young’s modulus parameters are the most important to be precisely described. In this sense the Chenoweth’s⁶⁴ and Mueller’s⁵¹ set of parameters would be the best choice. As Chenoweth⁶⁴ set was already used in Ref.⁴⁰ to investigate PG tensile strain tests, we decided to use Mueller’s set⁵¹ in our calculations, so we would have a good reference for comparisons.

MD results

In Figure 2 we present the PG stress-strain curve obtained from classical MD simulations based on the Mueller⁵¹ set of ReaxFF parameters. We observe two linear regimes, one elastic (regime 1) and the other a plastic one (regime 2) resulting from permanent deformations due to local structural reconstructions, as shown in Fig. 3. While the plastic regime starts at about 10% of strain, fracture takes place at about 20%, which is very close to the maximum of 21% of bi-axial tensile strain calculated by DFT.²⁹

In Figure 3a we present MD snapshots of PG strained structures, including one close to the moment of fracture, where the formation of many carbon chains can be seen. In Figures 3b-d we present representative MD snapshots of the plastic regime, where it is possible to observe the existence of 7, 8 and 11 carbon rings. These rings are formed from the reconstruction of broken $C - C$ bonds. In figure 4, we present representative MD snapshots showing the von Mises stress values of PG tensioned structures. Details of the carbon chains that are formed at large tension strains, just before final rupture of the structure, are shown in Fig. 5. The distances between the carbon atoms along the chains indicate the formation of a structure having single and triple bonds which is the so called polyynic configuration. This chain configuration has been predicted to be the most stable linear structure.

These results are quite different from those reported in Ref.,⁴⁰ which predicted that the

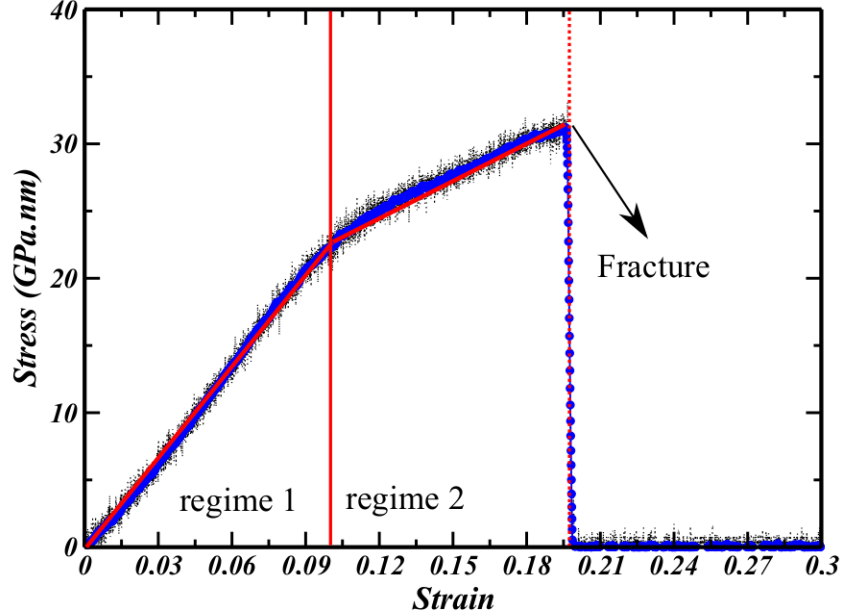


Figure 2: Pentagraphene (PG) stress-strain curve. Vertical red lines divide the curve into elastic (regime 1) and plastic (regime 2). Over-imposed red line on the stress-strain curve indicates the average inclinations in both regimes. Dashed vertical line indicates the maximum strain the system can stand before fracture.

PG structures evolve mostly to graphene-like conformations, during either tensile or thermal strains, although structural defects were also present. In our simulations, we did not observe the formation of hexagons during the tensile strains. The difference between our calculations and those reported in Ref.⁴⁰ is mainly the choice of the set of ReaxFF parameters. Ref.⁴⁰ used the Chenoweth⁶⁴ set of parameters while we used the Mueller⁵¹ one. From Table (1), and as discussed before, we see that the main differences between them are the results for the PG elastic modulus values. Chenoweth⁶⁴/(Mueller⁵¹) parameters provide softer (harder) PG structures than that predicted by DFT. For this reason, the harder structure predicted by Muller’s set can transform itself from pentagons directly to higher order rings, rather than to intermediate hexagons. This different results point out to the importance of a good choice of parameters in simulating the systems in order to prevent predictions that come out

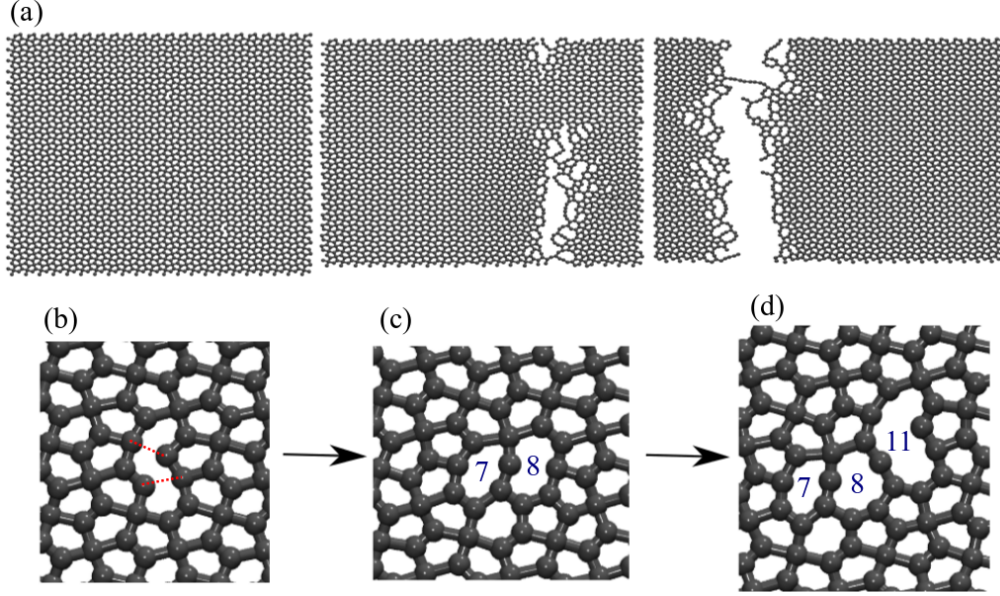


Figure 3: (a) Representative MD snapshots of tensioned PG structures at 0% (leftmost panel), 19.7% (middle panel) and 20% (rightmost panel) strains. (b), (c) and (d) are representative MD snapshots showing the existence of 7, 8, 11 rings formed at 18%, 18.5% and 18.7% tension strains.

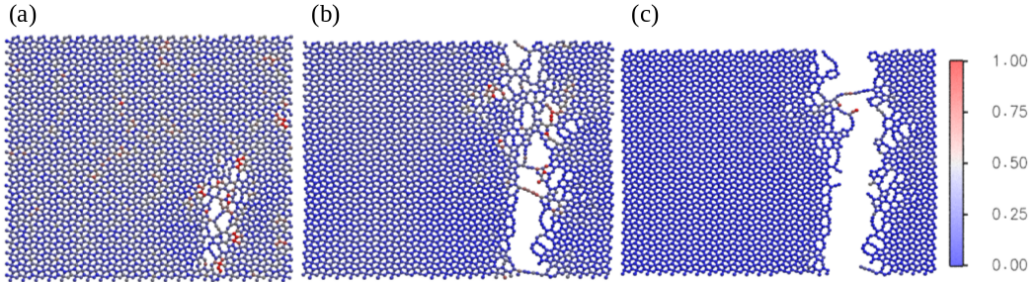


Figure 4: Representative MD snapshots showing the von Mises stress values of PG tensioned structures at (a) 19%, (b) 19.5% and (c) 20% strains.

from the unprecise description of the structure rather than from the physical behavior.

In order to gain further insights on which results are more realistic, we performed DFT calculations of the tensile strain up to fracture, as discussed next.

DFT results

We have carried out DFT calculations of PG structures under uniaxial and biaxial tensile strains up to limit of rupture. One of the goals of these calculations is to identify inter-

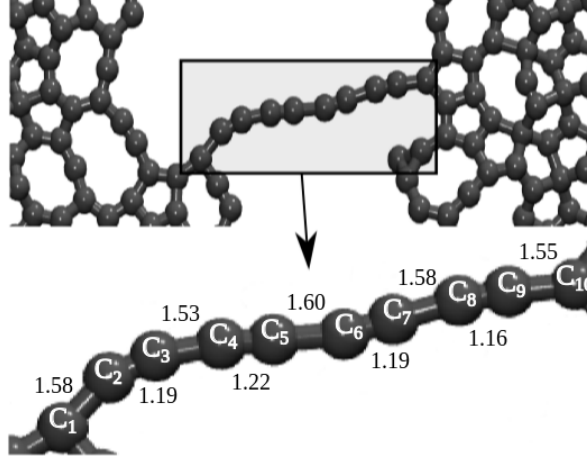


Figure 5: Structural details of a carbon chain formed at the last stages (before breaking) of a PG tensioned structure. Carbon atoms are labelled to identify the single and triple bonds that forms along the chain. Values in Angstroms.

mediate structures to help to understand the fracture dynamics. In addition, we want to get further insights on how suitable is the chosen set of ReaxFF parameters to describe the PG mechanical properties. Two orthogonal PG units cells were used in order to investigate differences in failure mechanisms. These units cells were labeled R0 and R45 (rotated of 45° from R0) as shown in Fig. 6a. It is interesting to note that R45 have neither perpendicular nor parallel C-C bonds along uniaxial x and y strains. However, R0 structure has both types of bonds, which will play a significant role just before the rupture under uniaxial strain. We have calculated the energy shift due to the in-plane strain to determine the PG mechanical stability. For a 2D membrane, using the standard Voigt notation (1- xx , 2- yy , and 6- xy), the elastic strain energy per unit area can be expressed as a function of C_{11} , C_{22} and C_{12} elastic modulus tensor, corresponding to second partial derivative of strain energy with respect to strain. The elastic constants can be derived by fitting the energy curves associated with uniaxial and equi-biaxial strains. The curves are plotted in Fig. 6b. We should note here that the mechanical behavior of R0 and R45 structures are almost the same in low-strain regime (up to 5%) producing similar results for the elastic constants. Under uniaxial strain, $\varepsilon_{yy} = 0$, $U(\varepsilon_{xx}) = 1/2C_{11}\varepsilon_{xx}^2$. Parabolic fitting of the uniaxial strain curve yields $C_{11} = 277.5$ GPa·nm. Under equi-biaxial strain, $\varepsilon_{yy} = \varepsilon_{xx}$, we have $U(\varepsilon_{xx}) = (C_{11} + C_{12})\varepsilon_{xx}^2$. By

fitting the equi-biaxial strain curve we obtain $C_{11} + C_{12} = 250.8 \text{ GPa}\cdot\text{nm}$, hence, $C_{12} = -26.7 \text{ GPa}\cdot\text{nm}$. The in-plane Young's modulus is calculated to be as large as $274.95 \text{ GPa}\cdot\text{nm}$, which is very similar to what was observed by other authors.²⁹ We also note that C_{12} is negative for this membrane, leading to a negative Poisson's ratio (NPR), $\nu = C_{12}/C_{11} = -0.096$. This result confirms that PG is an auxetic material. We also studied the ideal PG strength and failure mechanism by calculating the variation of stress as a function of the equi-biaxial and uniaxial tensile strain. The results are presented in Fig. 6c, which shows that the strain at the maximum stress before failure is 19.5% (uniaxial) and 23% (biaxial).

The simulation of uniaxial stretching loading with the in-plane perpendicular lattice vector fixed also allowed the computation of the residual perpendicular stress components (not shown in Fig. 6c), which exhibit negative values. Furthermore, when no constraints are imposed to uniaxial loading, the length of perpendicular lattice vectors increases. This result is an additional evidence that PG is an auxetic material. For equi-biaxial stretching loading, we plot $(\sigma_{xx} + \sigma_{yy})$ in Fig 6c. Therefore, we observed that the calculated ultimate tensile strength (UTS) shows that PG is very strong with the UTS of $\sim 38 \text{ GPa}\cdot\text{nm}$ (R0 uniaxial), and $\sim 29 \text{ GPa}\cdot\text{nm}$ (R45 uniaxial). This discrepancy will be further discussed. For biaxial stretching, we obtained UTS of $\sim 52 \text{ GPa}\cdot\text{nm}$ (biaxial) independent of the R0 or R45 conformation.

In Fig. 7a-b, we present PG snapshots for R0 and R45 structures, respectively before and after failure caused by a maximum of 20% for x -axis stretching (similar results were obtained for y -axis stretching, not shown). PG fractured membranes of Fig. 7a-b were duplicated along x - and y -direction in Fig 7c-d for a better visualization of the fracture patterns (see colored non-pentagonal rings). It is interesting to note that the patterns of R0 and R45 ruptured structures after 20% of strain are similar with the formation of porous membranes with $8 - C$ rings for both strained directions (cf. Fig. 7c-d). However, we note significant differences in R0 and R45 structures concerning the maximum of tensile stress under uniaxial stretching just before the rupture, as we can see in Fig. 6c. We obtained $\sim 38 \text{ GPa}\cdot\text{nm}$ (R0),

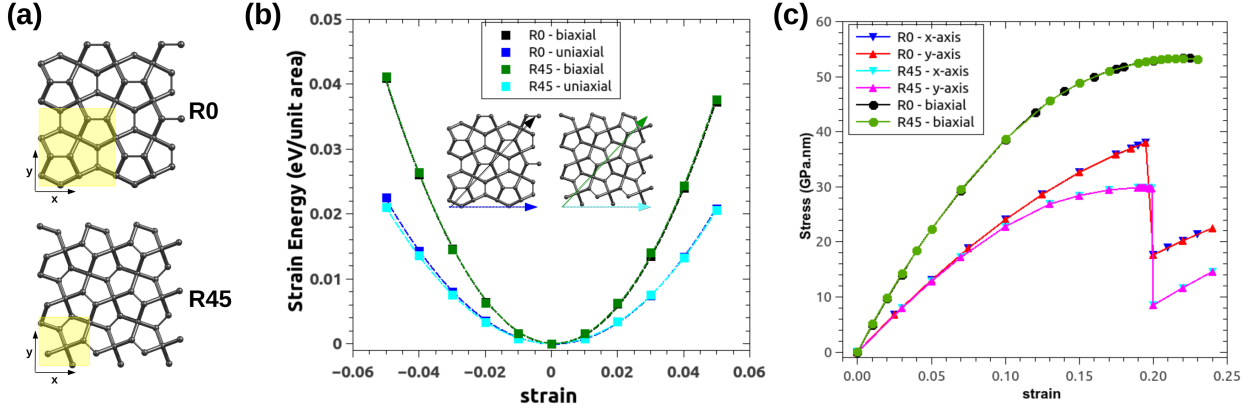


Figure 6: (a) R0 and R45 unit cells used to study pentagraphene (PG) failure mechanisms. The PG primitive cell (yellow square) was 2×2 (3×3) replicated for R0 (R45) structure in order to model the fracture process. (b) PG strain-energy curves in low-strain regime. Parabolic fitting was used to estimate the Young's modulus value (see text). (c) PG strain-stress curves for R0 and R45 under equi-biaxial and uniaxial stretching. Equi-biaxial (black and green) curves is $(\sigma_{xx} + \sigma_{yy})$ stress versus strain (ε_{xx}) . Uniaxial curves is $(\sigma_{xx})\sigma_{yy}$ versus $(\varepsilon_{xx}) \varepsilon_{yy}$ strain.

and $\sim 29\text{GPa.nm}$ (R45) for this quantity. We can explain such a difference in terms of the parallel C-C bonds present in R0 structure, which play a significant role at 19% of strain, as one can see in Fig. 8a.

For symmetry reasons, the original PG structure (no stressed) has only two types of C-C bonds, which connect both tri-coordinated atoms (1.33\AA) and also tri- and tetra-coordinated atoms (1.55\AA), independent of the R0 and R45 unit cell construction. However, when subjected to uniaxial loading, those bonds are stressed differently. At 19% of strain, the parallel aligned C-C bonds in R0 structure are stressed up to 1.46\AA , while the perpendicular C-C bonds remains with the same length of zero-strain structure, as we can observe in Fig. 8a (top panels). In R45 conformation, at 19% of strain, the same C-C bonds are slightly elongated to 1.37\AA . Therefore, we suggest that the triple coordinated carbon atoms connection in R0 structure are directed affected by uniaxial strain and this conformation causes a larger stress obtained for R0 conformation when compared to R45 structures. During the biaxial loading, as we can observe from Fig. 8b, similar C-C bond lengths are obtained for tri- and

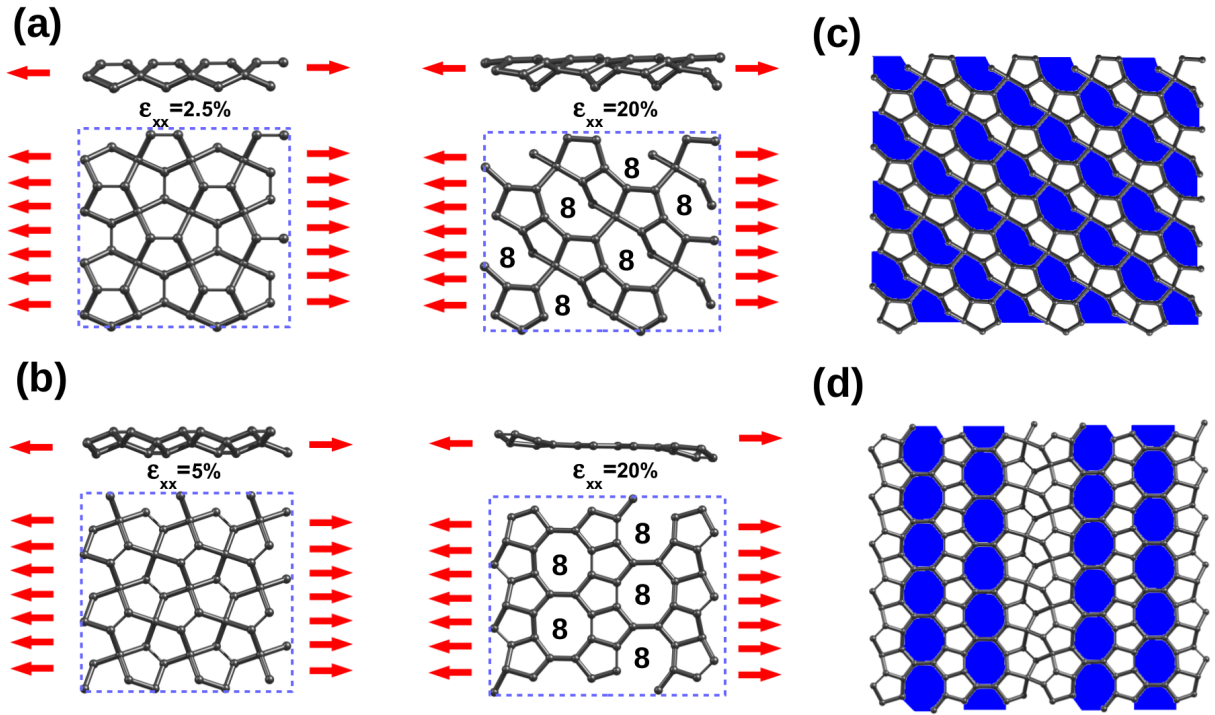


Figure 7: Snapshots of pentagraphene (PG) under 2.5% and 20% of uniaxial strain indicated by red arrows. (a) R0 structure after uniaxial stretching converges to 8-porous structures aligned to diagonal direction. A residual σ_{xy} stress component is obtained which indicated that those structure after the failure point is not energetically stable. (b) R45 structure after uniaxial stretching converges to 8-porous structures aligned to perpendicular direction. No residual σ_{xy} stress component are observed which indicated that those structure after failure point is energetically stable. Extended PG porous membranes after failure strain are also shown. Uniaxial strain of 20% along the x -axis for R0 structure (c) and R45 structure (d). Porous of 8 (blue) carbon atoms rings are highlighted for better visualization.

tetra-coordinated atoms, which can explain why stress-strain curves are very similar for R0 and R45 structure.

Our DFT results are closer to our MD simulations, rather than to those from reported in Ref.⁴⁰ Apart from differences related to temperature effects and sample size, the main reason for differences between the classical results lies in the softness of the material as predicted by the different simulation set parameters. Note that our MD prediction for Y and that from Ref.⁴⁰ are in opposite trends when compared to DFT. However, we observe

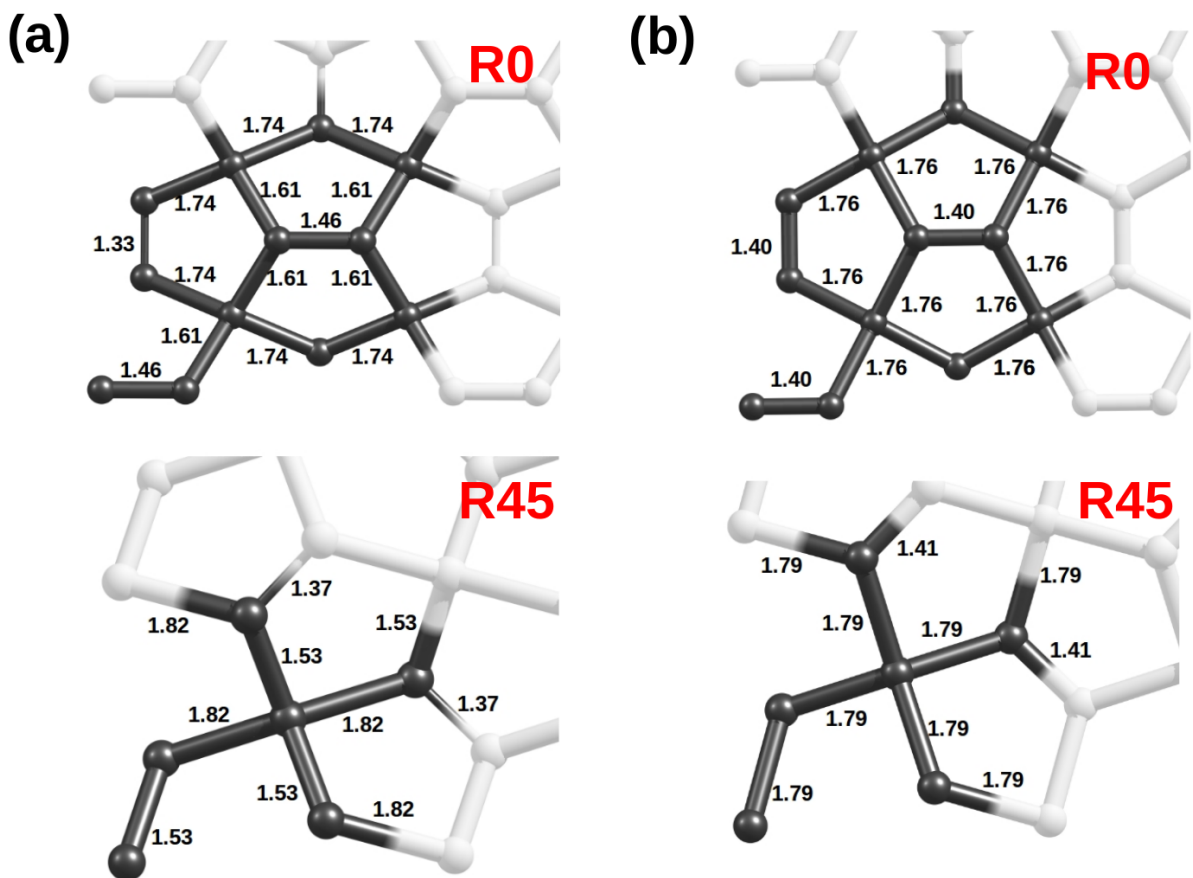


Figure 8: (a) R0 (top) and R45 (down) structures under 19% of uniaxial strain. (b) R0 (top) and R45 (down) structures under 19% of biaxial strain. Carbon-Carbon bonds lengths in Å units are shown in detail. Carbon atoms from primitive unit cell are highlighted in black for better visualization.

no hexagons during the fracture process (as investigated by DFT), which does not suggest a structural transition from PG to hexagraphene. This allows us to argue that the Muller's set of ReaxFF parameters is more suitable to describe the fracture of pentagraphene as its predictions are closer to what we expect from *ab initio* calculations.

Summary and Conclusions

In this work, we have investigated the mechanical properties and fracture patterns of a new carbon allotrope named pentagraphene (PG). We have combined DFT and reactive molecular dynamics simulations by using the well-known ReaxFF force field. Our results showed conflicting data depending on the set of parameters. DFT calculations help to explain these discrepancies and the Mueller's parameter set⁵¹ seems to provide more reliable results for this system. Our results also help to provide further insights on two conflicting literature issues regarding PG mechanical properties. The auxetic character (negative Poisson's ratio) was confirmed and the reported structural transition from PG to graphene⁴⁰ is not consistent with DFT results. We show that PG membranes can hold up to 20% of strain and that fracture occurs only after substantial dynamical bond breaking and the formation of 7, 8 and 11 carbon rings and carbon chains were observed prior complete fracture. The stress-strain behavior was observed to follow two regimes, one exhibiting linear elasticity followed by a plastic one, this one involving carbon atom re-hybridization with the formation of carbon rings and chains. Our MD results also show that mechanically induced structural transitions from PG to graphene is unlikely to occur, in contrast to what was previously predicted in the literature.

Acknowledgements

This work was supported in part by the Brazilian Agencies CAPES, CNPq and FAPESP. The authors thank the Center for Computational Engineering and Sciences at Unicamp for financial support through the FAPESP/CEPID Grant #2013/08293-7. AFF is a fellow of the Brazilian Agency CNPq (#302750/2015-0) and acknowledges support from FAPESP grant #2016/00023-9. ECG acknowledges support from Conselho Nacional de Desenvolvimento Científico e Tecnológico (CNPq) (Process Number 473714/2013-2). ECG and JMS acknowledge support from Coordenação de Aperfeiçoamento de Pessoal de Nível Superior (CAPES) through the Science Without Borders program (Project Number A085/2013). AGSF and JMS acknowledge PNPd CAPES fellowship.

References

References

- (1) K. S. A. Novoselov, A. K. Geim, S. V. Morozov, D. Jiang, M. I. Katsnelson, I. V. Grigorieva, S. V. Dubonos and A. A. Firsov, “Two-dimensional gas of massless Dirac fermions in graphene”, *Nature*, **438**, 197–200 (2005). DOI: 10.1038/nature04233
- (2) S. Park, R. S. Ruoff, “Chemical methods for the production of graphenes”, *Nat Nanotechnol* **4**, 217 (2009). DOI: 10.1038/nnano.2009.58.
- (3) W. Gao, L. B. Alemany, L. Ci, P. M. Ajayan, “New insights into the structure and reduction of graphite oxide”, *Nat Chem* **1**, 403 (2009). DOI: 10.1038/NCHEM.281.
- (4) S. Stankovich, D. A. Dikin, G. H. B. Dommett, K. M. Kohlhaas, E. J. Zimney, E. A. Stach, R. D. Piner, S. T. Nguyen, R. S. Ruoff, “Graphene-based composite materials”, *Nature* **442**, 282–286 (2006). DOI: 10.1038/nature04969
- (5) A. K. Geim, “Graphene: status and prospects” *Science* **324**, 1530–1534 (2009). DOI: 10.1126/science.1158877
- (6) H. Chen, M. B. Müller, K. J. Gilmore, G. G. Wallace, D. Li, “Mechanically strong, electrically conductive, and biocompatible graphene paper”, *Advanced Materials* **20**, 3557–3561, (2008). DOI: 10.1002/adma.200800757
- (7) G. Eda, M. Chhowalla, “Graphene-based composite thin films for electronics”, *Nano Letters*, **9**, 814–818 (2009). DOI: 10.1021/nl8035367
- (8) F. Scarpa, S. Adhikari, A. S. Phani, “Effective elastic mechanical properties of single layer graphene sheets”, *Nanotechnology* **20**, 065709 (2009). DOI: 10.1088/0957-4484/20/6/065709

- (9) F. Withers, M. Dubois, A. K. Savchenko, “Electron properties of fluorinated single-layer graphene transistors” *Physical Review B* **82**, 073403 (2010). DOI: 10.1103/PhysRevB.82.073403
- (10) Y. Xu, H. Bai, G. Lu, C. Li, G. Shi, “Flexible graphene films via the filtration of water-soluble noncovalent functionalized graphene sheets”, *Journal of the American Chemical Society* **130**, 5856–5857 (2008). DOI: 10.1021/ja800745y
- (11) T. Ramanathan, A. A. Abdala, S. Stankovich, D. A. Dikin, M. Herrera-Alonso, R. D. Piner, D. H. Adamson, H. C. Schniepp, X. Chen, R. S. Ruoff, *et al.*, “Functionalized graphene sheets for polymer nanocomposites”, *Nature Nanotechnology* **3**, 327–331 (2008). DOI: 10.1038/nnano.2008.96
- (12) Y. -W. Son, M. L. Cohen, S. G. Louie, “Half-metallic graphene nanoribbons”, *Nature* **444**, 347–349 (2006). DOI: 10.1038/nature05180
- (13) G. Giovannetti, P. A. Khomyakov, G. Brocks, P. J. Kelly, J. van den Brink, “Substrate-induced band gap in graphene on hexagonal boron nitride: Ab initio density functional calculations”, *Physical Review B* **76**, 073103 (2007). DOI: 10.1103/PhysRevB.76.073103
- (14) K. Watanabe, T. Taniguchi, H. Kanda, “Direct-bandgap properties and evidence for ultraviolet lasing of hexagonal boron nitride single crystal”, *Nature Materials* **3**, 404–409 (2004). DOI: 10.1038/nmat1134
- (15) P. Niu, L. Zhang, G. Liu, H. -M. Cheng, “Graphene-Like Carbon Nitride Nanosheets for Improved Photocatalytic Activities”, *Advanced Functional Materials* **22**, 4763–4770 (2012). DOI: 10.1002/adfm.201200922
- (16) A. Thomas, A. Fischer, F. Goettmann, M. Antonietti, J. -O. Müller, R. Schlögl, J. M. Carlsson, “Graphitic carbon nitride materials: variation of structure and morphology

- and their use as metal-free catalysts”, *Journal of Materials Chemistry* **18**, 4893–4908 (2008). DOI: 10.1039/B800274F
- (17) J. M. de Sousa, T. Botari, E. Perim, R. A. Bizardo and Douglas S. Galvao, “Mechanical and structural properties of graphene-like carbon nitride sheets”, *RSC Advances* **6**, 76915-76921 (2016). DOI: 10.1039/C6RA14273G
- (18) R. H. Baughman, H. Eckhardt, M. Kertesz, “Structure-property predictions for new planar forms of carbon: Layered phases containing sp² and sp atoms” *The Journal of Chemical Physics* **87**, 6687–6699 (1987). DOI: 10.1063/1.453405
- (19) V. R. Coluci, S. F. Braga, S. B. Legoas, D. S. Galvao, R. H. Baughman, “Families of carbon nanotubes: Graphyne-based nanotubes”, *Physical Review B* **68**, 035430 (2003). DOI: 10.1103/PhysRevB.68.035430
- (20) V. R. Coluci, S. F. Braga, S. B. Legoas, D. S. Galvao, R. H. Baughman, “New families of carbon nanotubes based on graphyne motifs”, *Nanotechnology* **15**, S142 (2004). DOI: 10.1088/0957-4484/15/4/006
- (21) A. L. Ivanovskii, “Graphynes and graphdiynes”, *Progress in Solid State Chemistry* **41**, 1 (2013). DOI: 10.1016/j.progsolidstchem.2012.12.001
- (22) Y. Li, L. Xu, H. Liu and Y. Li, “Graphdiyne and graphyne: from theoretical predictions to practical construction”, *Chem. Soc. Rev.* **43**, 2572 (2014). DOI: 10.1039/c3cs60388a
- (23) Q. H. Wang, K. Kalantar-Zadeh, A. Kis, J. N. Coleman, M. S. Strano, “Electronics and optoelectronics of two-dimensional transition metal dichalcogenides”, *Nature Nanotechnology* **7**, 699–712 (2012). DOI: 10.1038/nnano.2012.193
- (24) M. Chhowalla, H. S. Shin, G. Eda, L. -J. Li, K. P. Loh, H. Zhang, “The chemistry of two-dimensional layered transition metal dichalcogenide nanosheets”, *Nature Chemistry* **5**, 263–275 (2013). DOI:

- (25) K. Takeda, K. Shiraishi, “Theoretical possibility of stage corrugation in Si and Ge analogs of graphite” *Physical Review B* **50**, 14916 (1994). DOI: 10.1103/PhysRevB.50.14916
- (26) B. Aufray, A. Kara, S. Vizzini, H. Oughaddou, C. Leandri, B. Ealet, G. Le Lay, “Graphene-like silicon nanoribbons on Ag (110): A possible formation of silicene”, *Applied Physics Letters* **96**, 183102 (2010). DOI: 10.1063/1.3419932
- (27) P. Vogt, P. De Padova, C. Quaresima, J. Avila, E. Frantzeskakis, M. C. Asensio, A. Resta, B. Ealet, G. Le Lay, “Silicene: compelling experimental evidence for graphenelike two-dimensional silicon”, *Physical Review Letters* **108**, 155501 (2012). DOI: 10.1103/PhysRevLett.108.155501
- (28) H. Terrones, M. Terrones, E. Hernandez, N. Grobert, J. C. Charlier, P. M. Ajayan “New metallic allotropes of planar and tubular carbon” *Physical Review Letters* **84**, 1716–1719 (2000).
- (29) S. Zhang, J. Zhou, Q. Wang, X. Chen, Y. Kawazoe, P. Jena, “Penta-graphene: A new carbon allotrope”, *Proceedings of the National Academy of Sciences* **112**, 2372–2377 (2015). DOI: 10.1073/pnas.1416591112
- (30) R. H. Baughman and D. S. Galvao, “Crystalline networks with unusual predicted mechanical and thermal properties”, *Nature* **365**, 735–737 (1993). DOI: 10.1038/365735a0
- (31) C. P. Ewels, X. Rocquefelte, H. W. Kroto, M. J. Rayson, P. R. Briddon, M. I. Heggie, “Predicting experimentally stable allotropes: Instability of penta-graphene”, *Proceedings of the National Academy of Sciences* **112**, 15609–15612 (2015). DOI: 10.1073/pnas.1520402112
- (32) M. Yagmurcukardes, H. Sahin, J. Kang, E. Torun, F. M. Peeters, R. T. Senger, “Pentagonal monolayer crystals of carbon, boron nitride, and silver azide”, *Journal of Applied Physics* **118**, 104303 (2015). DOI: 10.1063/1.4930086

- (33) T. Stauber, J. I. Beltrn, J. Schliemann, “Tight-binding approach to pentagraphene”, *Sci. Reports* **6**, 22672 (2016). DOI: 10.1038/srep22672
- (34) W. Xu, G. Zhang, B. Li, “Thermal conductivity of penta-graphene from molecular dynamics study”, *The Journal of Chemical Physics* **143**, 154703 (2015). DOI: 10.1063/1.4933311
- (35) F. Q. Wang, J. Yu, Q. Wang, Y. Kawazoe, P. Jena, “Lattice thermal conductivity of penta-graphene”, *Carbon* **105**, 424–429 (2016). DOI: 10.1016/j.carbon.2016.04.054
- (36) B. Rajbanshi, S. Sarkar, B. Mandal, P. Sarkar, “Energetic and electronic structure of penta-graphene nanoribbons”, *Carbon* **100**, 118–125 (2016). DOI: 10.1016/j.carbon.2016.01.014
- (37) M. Yagmurcukardes, H. Sahin, J. Kang, E. Torun, F. M. Peeters, R. T. Senger, “Pentagonal monolayer crystals of carbon, boron nitride, and silver azide”, *J. Appl. Phys.* **118**, 104303 (2015). DOI: 10.1063/1.4930086
- (38) X. Li, S. Zhang, F. Q. Wang, Y. Guo, J. Liu, Q. Wang, “Tuning the electronic and mechanical properties of penta-graphene via hydrogenation and fluorination”, *Phys. Chem. Chem. Phys.* DOI: 10.1039/c6cp01092j
- (39) X. Wu, V. Varshney, J. Lee, T. Zhang, J. L. Wohlwend, A. K. Roy, T. Luo, “Hydrogenation of Penta-Graphene Leads to Unexpected Large Improvement in Thermal Conductivity”, *Nano Letters* DOI: 10.1021/acs.nanolett.6b01536
- (40) S. W. Cranford, “When is 6 less than 5? Penta- to hexa-graphene transition”, *Carbon* **96**, 421–428 (2016). DOI: 10.1016/j.carbon.2015.09.092
- (41) P. Hohenberg, W. Kohn, “Inhomogeneous Electron Gas”, *Phys. Rev.* **136**, B864 (1964). DOI: 10.1103/PhysRev.136.B864

- (42) W. Kohn, L. J. Sham, “Self-Consistent Equations Including Exchange and Correlation Effects”, *Phys. Rev. Lett.* **140**, A133 (1965). DOI: 10.1103/PhysRev.140.A1133
- (43) P. Ordejn, E. Artacho, J. M. Soler , “ Self-consistent order-N density-functional calculations for very large systems ”, *Phys. Rev. B* **53**, R10441 (1996). DOI: 10.1103/PhysRevB.53.R10441
- (44) D. Snchez-Portal, P. Ordejn, E. Artacho, J. M. Soler, “ Density-functional method for very large systems with LCAO basis sets ”, *International Journal of Quantum Chemistry* **65**, 453-461 (1997). DOI: 10.1002/(SICI)1097-461X(1997)65:5j453::AID-QUA9j3.0.CO;2-V
- (45) J. P. Perdew, K. Burke, M. Ernzerhof, “Generalized Gradient Approximation Made Simple”, *Phys. Rev. Lett.* **77**, 3865 (1996). DOI: 10.1103/PhysRevLett.77.3865
- (46) J. P. Perdew, K. Burke, M. Ernzerhof, “Efficient pseudopotentials for plane-wave calculations”, *Phys. Rev. B* **43**, 1993 (1991). DOI: 10.1103/PhysRevB.43.1993
- (47) L. Kleinman, D. M. Bylander, “Efficacious Form for Model Pseudopotentials”, *Phys. Rev. B* **48**, 1425 (1982). DOI: 10.1103/PhysRevLett.48.1425
- (48) H. J. Monkhorst, J. D. Pack, “Special points for Brillouin-zone integrations”, *Phys. Rev. B* **13**, 5188 (1976). DOI: 10.1103/PhysRevB.13.5188
- (49) E. Anglada, J. M. Soler, J. Junquera, E. Artacho, “Systematic generation of finite-range atomic basis sets for linear-scaling calculations ”, *Phys. Rev. B* **66**, 205101 (2002). DOI: 10.1103/PhysRevB.66.205101
- (50) A. C. T. Van Duin, S. Dasgupta, F. Lorant, W. A. Goddard, “ReaxFF: a reactive force field for hydrocarbons”, *The Journal of Physical Chemistry A* **105**, 9396–9409 (2001). DOI: 10.1021/jp004368u

- (51) J. E. Mueller, A. C. T. van Duin, W. A. Goddard III, “Development and validation of ReaxFF reactive force field for hydrocarbon chemistry catalyzed by nickel”, *The Journal of Physical Chemistry C* **114**, 4939–4949 (2010). DOI: 10.1021/jp9035056
- (52) S. Plimpton, “Fast parallel algorithms for short-range molecular dynamics”, *Journal of Computational Physics* **117**, 1–19 (1995). DOI: 10.1006/jcph.1995.1039
- (53) S. W. Cranford, M. J. Buehler, “Mechanical properties of graphyne”, *Carbon* **49**, 4111–4121 (2011). DOI: 10.1016/j.carbon.2011.05.024
- (54) T. Botari, E. Perim, P. A. S. Autreto, A. C. T. van Duin, R. Paupitz, D. S. Galvao, “Mechanical properties and fracture dynamics of silicene membranes”, *Physical Chemistry Chemical Physics* **16**, 19417–19423 (2014). DOI: 10.1039/C4CP02902J
- (55) N. Chen, M. T. Lusk, A. C. T. van Duin, W. A. Goddard III, “Mechanical properties of connected carbon nanorings via molecular dynamics simulation”, *Physical Review B* **72**, 085416 (2005). DOI: 10.1103/PhysRevB.72.085416
- (56) R. Mirzaeifar, Z. Qin, M. J. Buehler, “Tensile strength of carbyne chains in varied chemical environments and structural lengths”, *Nanotechnology* **25**, 371001 (2014). DOI: 10.1088/0957-4484/25/37/371001
- (57) A. K. Nair, S. W. Cranford, M. J. Buehler, “The minimal nanowire: Mechanical properties of carbyne”, *EPL (Europhysics Letters)* **95**, 16002 (2011). DOI: 10.1209/0295-5075/95/16002
- (58) M. Z. S. Flores, P. A. S. Autreto, S. B. Legoas, D. S. Galvao, “Graphene to graphane: a theoretical study”, *Nanotechnology* **20**, 465704 (2009). DOI: 10.1088/0957-4484/20/46/465704
- (59) P. A. S. Autreto, J. M. de Sousa, D. S. Galvao, “Site-dependent hydrogenation on graphdiyne” *Carbon* **77**, 829–834 (2014). DOI: 10.1016/j.carbon.2014.05.088

- (60) D. J. Evans, B. L. Holian, “The nose–hoover thermostat”, *The Journal of Chemical Physics* **83**, 4069–4074 (1985). DOI: 10.1063/1.449071
- (61) A. P. Garcia, M. J. Buehler, “Bioinspired nanoporous silicon provides great toughness at great deformability”, *Computational Materials Science* **48**, 303–309 (2010). DOI: 10.1016/j.commatsci.2010.01.011
- (62) R. P. B. Dos Santos, E. Perim, P. A. S. Autreto, G. Brunetto, D. S. Galvao, “On the unzipping of multiwalled carbon nanotubes”, *Nanotechnology* **23**, 465702 (2012). DOI: 10.1088/0957-4484/23/46/465702
- (63) T. R. Mattsson, J. M. D. Lane, K. R. Cochrane, M. P. Desjarlais, A. P. Thompson, F. Pierce, G. S. Grest, “First-principles and classical molecular dynamics simulation of shocked polymers”, *Physical Review B* **81**, 054103 (2010). DOI: 10.1103/PhysRevB.81.054103
- (64) K. Chenoweth, A. C. T. van Duin, W. A. Goddard III, “ReaxFF Reactive Force Field for Molecular Dynamics Simulations of Hydrocarbon Oxidation” *J. Phys. Chem. A* **112**, 1040–1053 (2008). DOI: 10.1021/jp709896w.
- (65) S. G. Srinivasan, A. C. T. van Duin, P. Ganesh, “Development of a ReaxFF Potential for Carbon Condensed Phases and its Application to the Thermal Fragmentation of a Large Fullerene”, *The Journal of Physical Chemistry A* **119**, 571–580 (2015). DOI: 10.1021/jp510274e